FUNCTIONAL BEAMFORMING

Robert P. Dougherty[1]
[1]OptiNav, Inc.
1414 127th PL NE #106, 98004, Bellevue, WA, USA

ABSTRACT

A new beamforming algorithm is introduced. It is called Functional Beamforming because it uses the mathematics of functions of matrices. The algorithm depends on an exponent parameter. The array Cross Spectral Matrix is raised to the power of the reciprocal of this exponent in the functional sense. Conventional Frequency Domain Beamforming is applied using the modified CSM, and the values of the resulting beamform map are raised to power of the non-reciprocal exponent. For large values of the exponent, array sidelobes are essentially eliminated. This increases flexibility in array design and dramatically increases the dynamic range of the system so that new sources may be discovered. Theory is given that proves that the method will not eliminate or even reduce true sources if the steering vector is accurate. This depends on the quality the array calibration, but the requirements are not extraordinary. Examples are given comparing the method with Robust Adaptive Beamforming, CLEAN-SC, Orthogonal Beamforming, and to some degree, Linear Programming. A previously unknown noise source of Boeing 747 desk models is shown.

1 INTRODUCTION

For many years, beamforming in acoustics and other fields has made use of sparse arrays in order to obtain acceptable results over a wide frequency range with a constrained number of sensors. Conventional beamforming (Frequency Domain Beamforming, FDBF) produces image maps with high sidelobe levels and severely limited dynamic range. Deconvolution methods have been applied to post process the complete maps [1,2] or decompose the cross spectral matrix into parts due to individual sources [3-5]. These methods can increase the dynamic range to some degree, but also can introduce new problems by replacing continuous source distributions with misleading spots. In some cases they are computationally expensive, requiring rooms full of computers to be employed in the processing. Adaptive beamforming formulas are popular in underwater acoustics [6-8] but have seen limited use in aeroacoustics and noise control. Difficulties with sidelobes continue to drive users of phased arrays to high channel counts, resulting in expensive systems, complicated tests, and elaborate processing. Poor dynamic range means that weak sources will be overlooked. This may not be obviously critical in noise control work, where the loudest source is the biggest problem, but there are

other applications of phase arrays where the weak sources are interesting. The ultimate example may radio astronomy.

1.1   Notation and goal

The model begins with a distribution of M mutually incoherent sources with strengths s_j, $j = 1,…, M$. They are usually considered to be monopoles, but could also be something else, such as duct modes, wavepackets, or a combination of source types. There are N microphones in the phased array. The array cross spectral matrix (CSM) is assumed to be given by

$$\mathbf{C} = \sum_{j=1}^{M} s_j \boldsymbol{g}_j \boldsymbol{g}'_j \qquad (1)$$

where the N-vector $\boldsymbol{g}_j$ is the array steering vector for source j. The normalization of steering vectors is $\boldsymbol{g}'_j \boldsymbol{g}_j = 1$.

The additional incoherent noise term that is usually assumed in a model like Eq. 1 is omitted on the basis that any such noise has been removed by a CSM diagonal optimization procedure. The method is beyond the scope of this paper, but the idea is to replace the diagonal elements of the CSM so as to minimize the trace subject to the constraint that **C** is non-negative definite. This is formulated as a sequence of linear programming problems, where the constraint matrix grows as eigenvectors of the matrices using trial solutions are computed. It turns out to be a fast, simple computation.

The beamforming problem is to determine the values of the s_j from a measurement of **C**. The $\boldsymbol{g}_j$ are assumed to be known. This assumption is less restrictive than it might seem because M can be taken to be very large. Presumably many of the s_j are actually 0.

The FDBF expression is

$$b(\boldsymbol{g}) = \boldsymbol{g}'\mathbf{C}\boldsymbol{g}. \qquad (2)$$

This expression is employed by replacing **g** with each of the grid steering vectors $\mathbf{g}_j$ in turn, to create the beamform map $b_j = b(\mathbf{g}_j)$, $j = 1, M$. To examine the performance of this expression, assume initially that only one of the s_j is nonzero. Let this be source number k. Then

$$\mathbf{C} = s_k \boldsymbol{g}_k \boldsymbol{g}'_k \qquad (3)$$

and steering to the correct location gives $b(\boldsymbol{g}_k) = s_k \boldsymbol{g}'_k \boldsymbol{g}_k \boldsymbol{g}'_k \boldsymbol{g}_k = s_k$. Moving to a general location with steering vector $\boldsymbol{g}$ produces $b(\boldsymbol{g}) = s_k \boldsymbol{g}' \boldsymbol{g}_k \boldsymbol{g}'_k \boldsymbol{g} = s_k |\boldsymbol{g}' \boldsymbol{g}_k|^2$. The factor $|\boldsymbol{g}' \boldsymbol{g}_k|^2$ is, of course, the array point spread function (PSF). It is less than or equal to unity, reaching 1 at the correct source location and any alias points. As $\boldsymbol{g}$ is moved away from $\boldsymbol{g}_k$, the values of the PSF decreases slowly at first, eventually describing the beamforming peak shape. Near the peak, the PSF can be interpreted as $cos^2\theta$, where θ is the angle between **g** and $\boldsymbol{g}_k$ in the N-dimensional steering vector space. Outside the peak, the PSF of a typical sparse array at high frequency has numerous sidelobes with levels of about -7 to -10 dB [7,9]. This level characterizes the dynamic range of FDBF with a single source.

Suppose there are multiple sources and let one of interest, number k again, be symbolically segregated from the others by writing

$$\mathbf{C} = s_k \boldsymbol{g}_k \boldsymbol{g}'_k \ + \mathbf{D} \tag{4}$$

where

$$\mathbf{D} = \sum_{j \neq k} s_j \boldsymbol{g}_j \boldsymbol{g}'_j. \tag{5}$$

Applying FDBF for location k gives

$$b(\boldsymbol{g}_k) \ = \ s_k + \boldsymbol{g}'_k \mathbf{D} \boldsymbol{g}_k. \tag{6}$$

By Eq. 5, $\mathbf{D}$ is a non-negative definite Hermitian matrix. This means $\boldsymbol{g}'_k \mathbf{D} \boldsymbol{g}_k \geq 0$ and $b(\boldsymbol{g}_k) \geq s_k$. The FDBF expression is a lower bound on the value of the source at the location corresponding to the steering vector. The amount by which the beamforming result exceeds the correct value depends on the other sources, $\mathbf{D}$, and the effect of the PSF on them. If the other sources are much stronger than s_k, then $\boldsymbol{g}'_k \mathbf{D} \boldsymbol{g}_k$ can dominate Eq. (6) and the s_k can be overlooked in the beamform map.

2   THE FUNCTIONAL BEAMFORMING FOMULA

2.1   Motivation and map of order 2

Let the spectral decomposition of $\mathbf{C}$ be written

$$\mathbf{C} = \ \mathbf{U} \mathbf{\Sigma} \mathbf{U}' \tag{7}$$

where $\mathbf{U}$ is a unitary matrix whose columns, $\boldsymbol{u}_1$, …, $\boldsymbol{u}_N$, are the eigenvectors of $\mathbf{C}$ and $\mathbf{\Sigma} = \mathrm{diag}(\sigma_1, \dots, \sigma_N)$ is a diagonal matrix whose diagonal elements are the eigenvalues. Let f be a function defined on $[0, \infty)$. A function of $\mathbf{C}$ is defined by [10]

$$f(\mathbf{C}) = \ \mathbf{U} f(\mathbf{\Sigma}) \mathbf{U}' = \ \mathbf{U} \, \mathrm{diag}[f(\sigma_1), \dots, f(\sigma_N)] \, \mathbf{U}' \tag{8}$$

which is to say the function is applied to the eigenvalues.

Let $f(t) = t^{\frac{1}{2}}$. Then the square root of the CSM becomes

$$\mathbf{C}^{\frac{1}{2}} = \mathbf{U} \mathrm{diag}\left(\sigma_1^{\frac{1}{2}}, \dots, \sigma_N^{\frac{1}{2}} \right) \mathbf{U}'. \tag{9}$$

An interesting vector related to the beamform map can be defined by

$$\boldsymbol{h}(\boldsymbol{g}) = \mathbf{C}^{\frac{1}{2}} \boldsymbol{g}. \tag{10}$$

In terms of $\boldsymbol{h}$, the FDBF is expression is

$$b(\boldsymbol{g}) = \boldsymbol{h}' \boldsymbol{h}. \tag{11}$$

If j_1 and j_2 are two different points in the grid and $\boldsymbol{h}_{j_1} = \mathbf{C}^{\frac{1}{2}} \boldsymbol{g}_{j_1}$ and $\boldsymbol{h}_{j_2} = \mathbf{C}^{\frac{1}{2}} \boldsymbol{g}_{j_2}$ then

$$\boldsymbol{h}'_{j_1} \boldsymbol{h}_{j_2} = \boldsymbol{g}'_{j_1} \mathbf{C} \boldsymbol{g}_{j_2} \tag{12}$$

is the source cross power between the two points [3].

In addition to Eq. (11), another way to produce a scalar map from the vector map $\boldsymbol{h}$ is to take the inner product with $\boldsymbol{g}$:

$$w(\boldsymbol{g}) = \boldsymbol{g}' \boldsymbol{h} = \boldsymbol{g}' \mathbf{C}^{\frac{1}{2}} \boldsymbol{g} \tag{13}$$

This function $w(\boldsymbol{g})$ is sufficiently related to the FDBF map that it is worth exploring its form in the case of a single source. Suppose the CSM is given by Eq. 3. Since this **C** is rank-1, it only has one nonzero eigenvalue, $\sigma_1 = s_k$, and the corresponding eigenvector is the steering vector: $\boldsymbol{u}_1 = \boldsymbol{g}_k$. For a single source, Eq. 13 then reduces to

$$w(\boldsymbol{g}) = s_k^{\frac{1}{2}} |\boldsymbol{g}' \boldsymbol{g}_k|^2. \tag{14}$$

This is identical to the FDBF map result for a single source, with the exception that it is proportional to the square root of the source strength, rather than the full source that appears in the FDBF expression. The PSF is identical to the FDBF case. In order to transform this map into an estimate of the source strength, it is necessary to square it. This will produce the expected result, s_k, when steering to $\boldsymbol{g} = \boldsymbol{g}_k$. If $\boldsymbol{g}$ corresponds to the location of a sidelobe, a spurious peak in $|\boldsymbol{g}' \boldsymbol{g}_k|^2$ for some $\boldsymbol{g}$ remote from $\boldsymbol{g}_k$, then squaring $w(\boldsymbol{g})$ will square the value of the PSF at the sidelobe. But, unless the sidelobe is an alias, the PSF is less than one at that point, so squaring the value will make it smaller. If the sidelobe level is -7 dB, then squaring $w(\boldsymbol{g})$ to produce the source strength estimate with give a new sidelobe level of -14 dB. The same observation applies to steering vectors that are within the main peak near point k: the peak will be sharpened. The effect of squaring will be small for points that are very close to the source, since $cos^2\theta$ is close to 1 in this case.

With this motivation, let the Functional Beamforming (FB) map of order 2 by defined by

$$b_2(\boldsymbol{g}) = \left[\boldsymbol{g}' C^{\frac{1}{2}} \boldsymbol{g} \right]^2. \tag{15}$$

It has been shown that, for single sources, this map produces the correct source strength and has twice the dynamic range and somewhat better resolution compared with FDBF. Computation time is essentially identical to FDFB, since the only significant addition to the effort is the spectral decomposition of the CSM, and this is faster that the other operations in beamforming.

2.2 Functional beamforming expression

Equation 15 and the action of the exponent on the sidelobes suggests a generalization:

$$b_\nu(\boldsymbol{g}) = \left[\boldsymbol{g}'\mathbf{C}^{\frac{1}{\nu}}\boldsymbol{g}\right]^\nu .$$ (16)

This is the Functional Beamforming map of order ν. It is useful for $\nu \geq 1$. Typical values of ν are in the range of 20-300. It reduces to FDBF for $\nu = 1$. Oddly, it produces the MVDR (minimum variance distortionless response) beamformer for $\nu = -1$.

For a single source, the reasoning above for $\nu = 2$ applies to the general case: $b_\nu(\boldsymbol{g_k}) = s_k$ and the sidelobes of the PSF will be suppressed, as the (standard) PSF is raised to the power ν in the last step of the calculation. If, for example, $\nu = 100$ and the array has a peak sidelobe level of -7 dB, then the Functional Beamforming sidelobe level for a single source will be -700 dB. Functional Beamforming essentially eliminates sidelobes for single sources. It also sharpens the peak for single sources. Numerical experiments show that it improves the resolution of multiple, closely spaced, sources relative to FDBF, but not dramatically so.

2.3   Inequalities governing performance with multiple sources

Expressed in terms of the eigenvalues of $\mathbf{C}$, the functional beamforming formula is

$$b_\nu(\boldsymbol{g}) = \left[\sum_{i=1}^{N} a_i \sigma_i^{\frac{1}{\nu}}\right]^\nu$$ (17)

where

$$a_i = |\mathbf{g}'\mathbf{u}_i|^2, \qquad i = 1, \dots, N$$ (18)

and

$$\sum_{i=1}^{N} a_i \;\; = 1.$$ (19)

Expression (17) is a weighted power mean of the eigenvalues with weights a_i. The weighted power means inequality [11] states that $b_\nu(\boldsymbol{g})$ is a non-increasing function of ν, and is strictly decreasing unless all of the eigenvalues are equal. The limiting value is a weighted geometric mean

$$\lim_{\nu \to \infty} b_\nu(\mathbf{g}) = \prod_{i=1}^{N} \sigma_i^{a_i}$$ (20)

but this expression is probably too unstable for use in practice as it stands.

Returning to Eq. (4), suppose there is a source with strength s_k at point k and that the other sources make a contribution $\mathbf{D}$ to the CSM. Consider two CSMs, $\mathbf{K} = s_k \boldsymbol{g_k}\boldsymbol{g}_k'$ and $\mathbf{C} = \mathbf{K} + \mathbf{D}$. These obey the inequality $\mathbf{C} \geq \mathbf{K}$ where this inequality is defined for Hermitian matrices to mean that $\mathbf{C} - \mathbf{K}$ has no negative eigenvalues, or equivalently, that $\boldsymbol{g}'(\mathbf{C} - \mathbf{K})\boldsymbol{g} \geq 0$ for all $\boldsymbol{g}$. Evaluating this with $\boldsymbol{g} = \boldsymbol{g_k}$ again proves that the FDBF result is greater than or equal to the true source strength.

If **A** and **B** are nonnegative definite matrices and $\mathbf{A} \geq \mathbf{B}$ then the Löwner-Heinz inequality [10] states that $\mathbf{A}^r \geq \mathbf{B}^r$ for $0 \leq r \leq 1$. Applying this to the present case shows that $\mathbf{C}^{\frac{1}{\nu}} \geq \mathbf{K}^{\frac{1}{\nu}}$ for $\nu \geq 1$. Using this in Eq. 16 proves that $b_\nu(\boldsymbol{g}_k) \geq s_k$.

The two inequality results show that $b_\nu(\boldsymbol{g}_k)$ is always greater than or equal to the true source strength at point k, and that $b_\nu(\boldsymbol{g}_k)$ is monotonically decreasing as ν increases (except in the pathological case that all of the eigenvalues are equal.) Taken together, these suggest that Functional Beamforming may converge to the correct answer for large ν. Future work is required to determine whether limiting value, Eq. 20, is always equal to s_k. This is clearly the case if $\boldsymbol{g}_k$ is an eigenvector of **C**.

2.4   Effect of errors in the steering vectors

In the formulas above, it has been assumed that exact steering vectors $\boldsymbol{g}$ can be produced for the potential sources. This is not a problem for simulations, but simulated results may overestimate the performance of the method with real data. If a given source has an actual steering vector $\boldsymbol{g}_a$ and the closest steering vector computed for the beamforming is $\boldsymbol{g}_m$ then the value of the PSF that will be used in the beamforming at the closest grid point is $cos^2\theta = |\boldsymbol{g}_m'\boldsymbol{g}_a|^2$. Applying FB of order ν, the error in the steering vector will reduce the value of the beamform map by a factor of $cos^{2\nu}\theta = |\boldsymbol{g}_m'\boldsymbol{g}_a|^{2\nu}$. For small θ, Bernouli's inequality [11] gives

$$cos^{2\nu}\theta \approx \left(1 - \frac{\theta^2}{2}\right)^{2\nu} \geq 1 - 2\nu\theta^2. \tag{21}$$

If ν is small enough that $2\nu\theta^2 \ll 1$, then the peak value of the PSF will still be close to 1, even after raising the map to the power ν in functional beamforming. If $2\nu\theta^2$ approaches 1, then the peaks of the functional beamforming maps are likely to be degraded. This means that array calibration is crucial for functional beamforming. Flawed calibration (or a grid that is too coarse or an incorrect physical model for $\boldsymbol{g}$) will set a certain minimum value for θ, and this in turn will limit the maximum value of ν that can be used before the peak values begin to plunge as ν is further increased. This is a problem because it limits the ability to take advantage if the power of functional beamforming in dynamic range and resolution. In practice, the upper limit for ν for a given dataset and steering vector model can be found by increasing ν until the peaks corresponding to true sources begin to fall off significantly. (The sidelobes will decrease dramatically, of course, and the true peaks may fall slightly at first as ν is increased from 1 because of removal of contamination from other sources. The limiting value of ν is indicated by a continuing, large, decrease in the physical peaks.)

3   EXAMPLES

Several example are given to illustrate the properties of FB and its relationship to other methods: FDBF, CLEAN-SC [3] Orthogonal Beamforming (OB) [5], Robust Adaptive Beamforming (RAB) [6-8], and Linear Programming [2].

3.1   Example setup and initial results

Most of the examples were produced using Array 24 Jr. (Fig. 1), which has 24 inexpensive electret microphones arranged in a non-redundant planar pattern with a diameter of

approximately 0.35m. The measurements were made in a warehouse laboratory with some foam rubber absorber arranged on floor and on partitions to reduce some of the acoustic reflections during the speaker calibration and the measurements.

Fig. 1. Array 24 Jr set up for the jet noise test. The 24 microphones are arranged in a 0.35 m pattern. The jet speed is Mach 0.15.

The microphone pattern of Array 24 Jr was used compute a synthetic CSM for a 0.5 m line of 1000 incoherent monopoles parallel to the array at distance of 3 m. Results at 20 kHz using FDBF, FB with $\nu = 20$ and $\nu = 200$, RAB with diagonal loading factor $\lambda = 0.01$ (see [8]), CLEAN-SC with a safety factor of 0.1, and OB with 23 eigenvalues are shown in Fig. 2. It is seen that, in this simulated case, Functional Beamforming has good resolution, dynamic range, and smoothness with this distributed source, and none of the other methods do. Specifically, FDBF has smoothness but poor dynamic range and resolution. RAB has smoothness, good resolution, and modestly improved dynamic range compared with FDBF. CLEAN-SC and OB have resolution and appear to exhibit dynamic range in this case, but do not give smooth results.
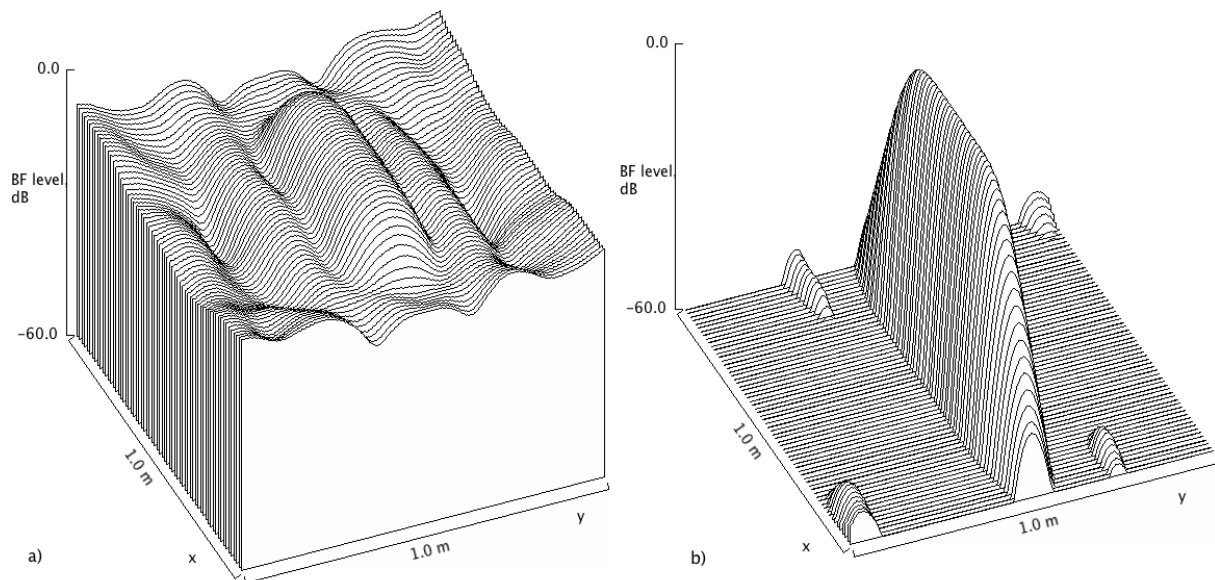
Fig. 2 a) and b). Beamforming results from a simulated line source of length 0.5 m placed 3m from Array 24 Jr. a) FDBF, b) Functional beamforming with $\nu = 20$. 20 kHz.
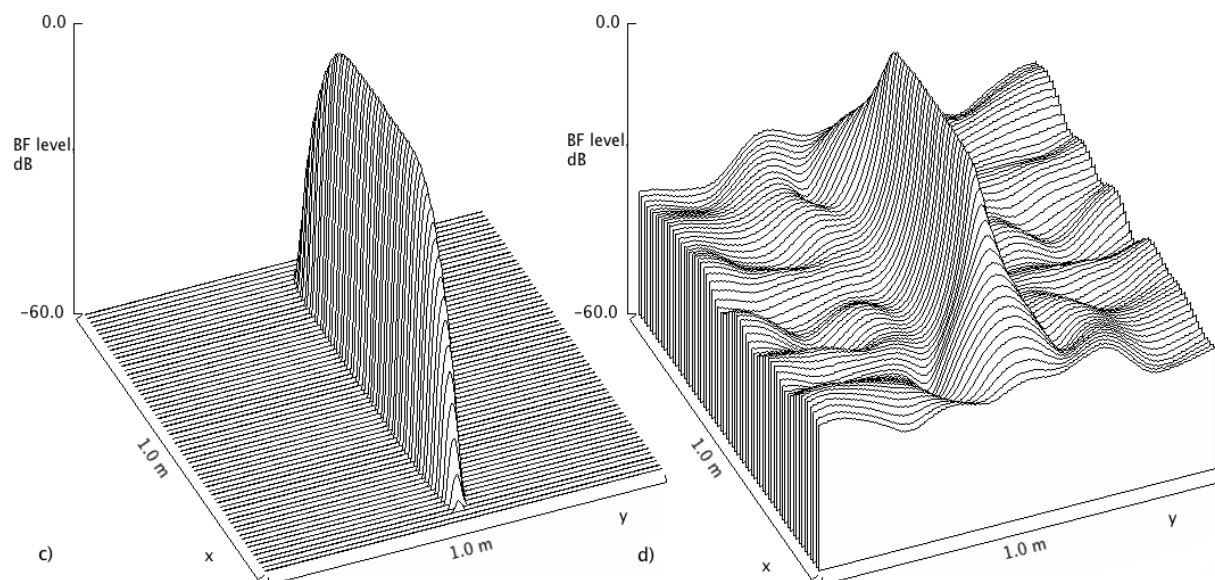
Fig. 2 c) and d). Beamforming results from a simulated line source of length 0.5 m placed 3m from Array 24 Jr. c) Functional beamforming with $\nu = 200$, d) Robust Adaptive Beamforming with $\lambda = 0.01$ in the notation of Huang et al [8]. 20 kHz.
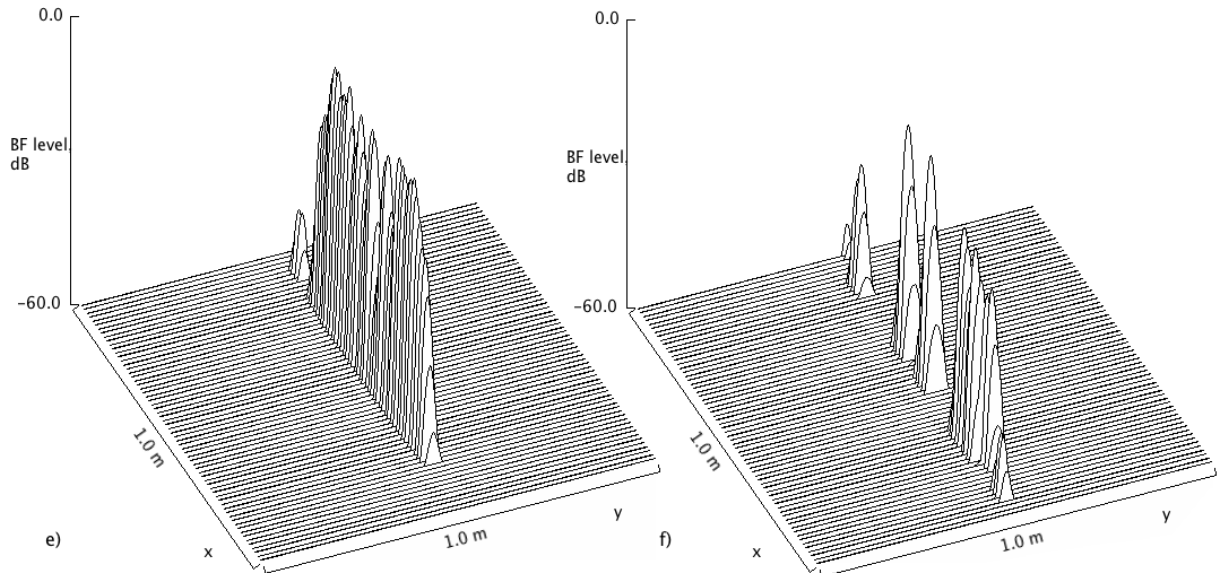
Fig. 2 e) and f). Beamforming results from a simulated line source of length 0.5 m placed 3m from Array 24 Jr. e) CLEAN-SC with safety factor $\varphi = 0.1$. f) Orthogonal Beamforming with 23 of the possible 24 eigenvectors used. 20 kHz.

A small speaker was placed on a table 3 m from Array 24 Jr (at $x = 0$), driven with white noise, and used to record array data. The speaker was then moved laterally by 0.2 m and a second dataset was measured. This data from $x = 0.2$ m was used as the speaker calibration for the preparation of Figs. 3-5. The speaker was then moved to $x = 0.5$ m and a third dataset was recorded. Results from processing the data from $x = 0$ are given in Figs. 3 and 4. Figure 5 combines data from the 0 m and 0.5 m positions.

Figure 3a)-c) gives results for the speaker at $x = 0$ processed using FDBF and plotted using 10, 20, and 60 dB scales. The result of FB with $\nu = 100$ is shown on the 60 dB scale in Fig. 3d). Sparse-array sidelobes as high as -6.5 dB can be seen in Fig. 3a). The first Airy ring from the generally round shape of the aperture and more details of the sidelobes are seen in Fig. 3b). More sidelobes and general floor of the pattern at about -30 dB are seen in Fig. 3c). The highest sidelobe in Fig. 3d) is -40.9 dB. Increasing ν to 200 (not shown) decreases the highest sidelobe to -50.8 dB. Decreasing ν to 30 (not shown) increases the highest sidelobe to -30 dB.
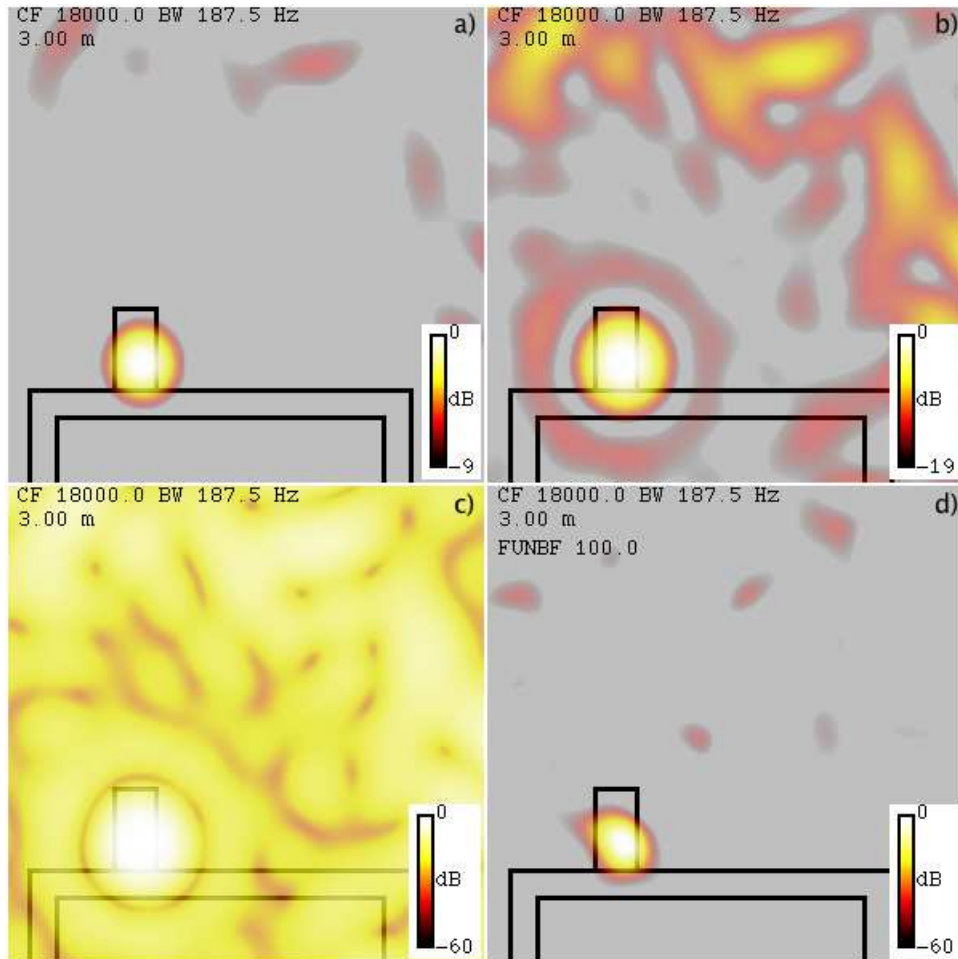
Fig. 3. Beamforming at 18 kHz for a speaker located 3 m from Array 24 Jr. a) FDBF on a 10 dB scale. b) FDBF on a 20 dB scale. c) FDBF on a 60 dB scale. d) Functional Beamforming with $\nu = 100$ on a 60 dB scale. Speaker calibration was applied using the same speaker in a different location.

Figure 3 is scaled to show the peak at 0 dB. The effect of ν on the peak level before scaling is shown in Fig. 4a) for the case with speaker calibration and 4b) for no speaker calibration. The limiting value of ν in the calibrated case is seen to be close to 200. The peak reduction effect is smaller at higher frequency, possibly because the array diffraction effects, which presumably compromise the calibration, are weaker at higher frequency. FB can still be applied without speaker calibration, but, as indicated in Fig. 4b) the useful value of ν is more limited. Fig. 4b) suggests that of ν can be 30 or possibly higher for frequencies up to 12 kHz, but at higher frequency ν should be constrained to values less than 30 in the case with no calibration. In contrast with the calibrated case, the peak level falls off faster with ν at high frequency. This may be because there are phase and amplitude errors in the microphones, and such errors are more important at high frequency. It should be noted that the electrets in Array 24 Jr have considerable variation in sensitivity between them. This should be viewed as nearly a worst-case array to use without calibration. A worse case would be to mount the microphones on wobbly stands and fail to measure their exact locations.
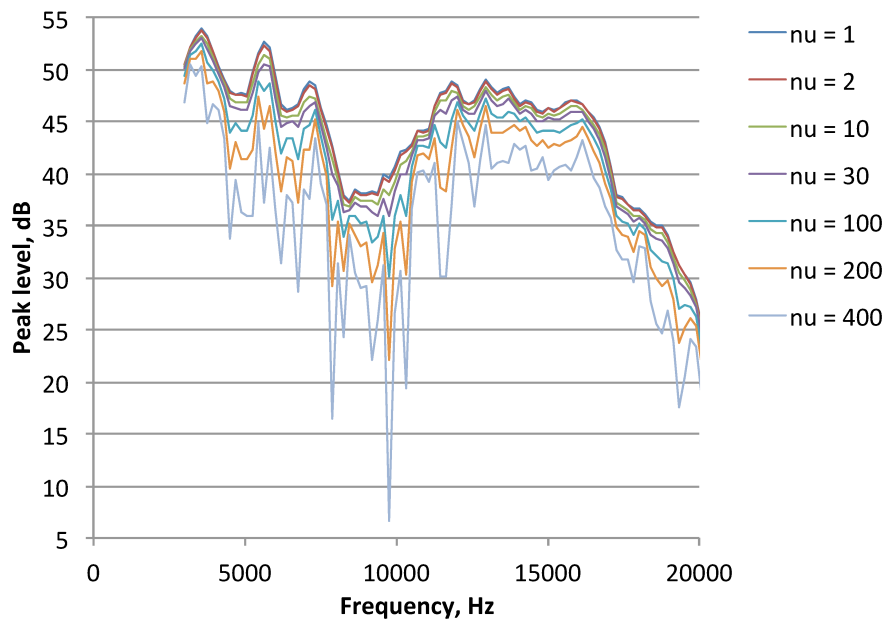
Fig. 4a. The effect of the Functional Beamforming order, ν, on the beamforming peak level. Speaker data and Array 24 Jr. The same speaker in a different position was used for calibration.
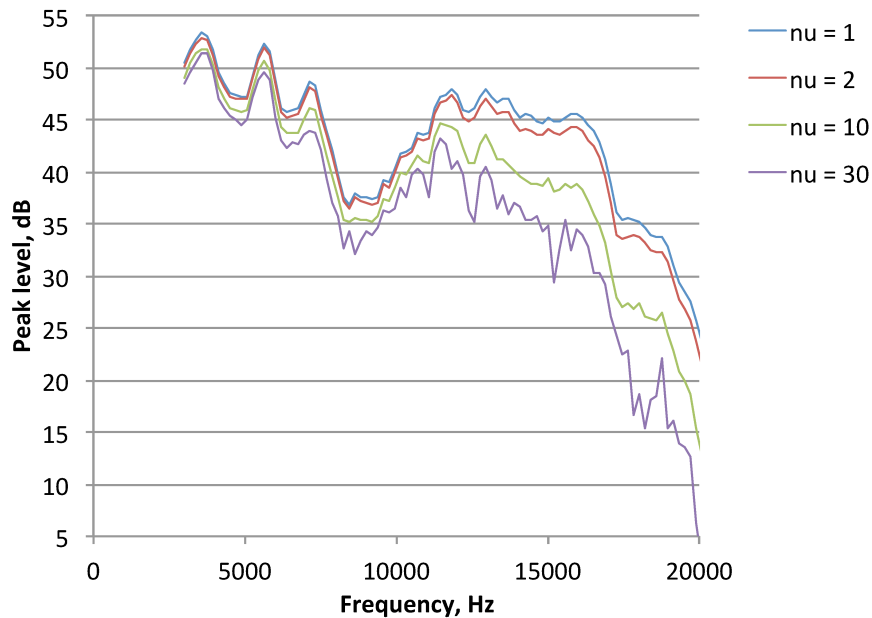

Fig. 4b. The effect of the Functional Beamforming order, ν, on the beamforming peak level. Speaker data and Array 24 Jr. No speaker calibration.

3.2 Resolution test

The CSM from the speaker data from $x = 0.5$ m was divided by 2 and added to the CSM from $x = 0$. This produced a CSM representing two incoherent sources with a separation of 0.5 m and a source level difference of 3 dB at a distance of 3 m from the array. Results for

11

FDBF, RAB, CLEAN-SC, OB, LP, and FB are given in Fig. 5a)-f). The Sparrow limit frequency [2] for the 0.5 m spacing is 3880 Hz and the Rayleigh limit frequency is 5030 Hz, but neither limit is strictly appropriate for the unequal source strengths. FDBF separated the sources at 6187 Hz. The order ν for FB was set at 50 to control scatter in the relative source strength and keep the weaker source in the 10 dB plot scale. With this setting, FB separated the sources at 4875 Hz. RAB just barely separated the sources at 3187 Hz. OB has bias error at low frequency and places the sources accurately at about 4687 Hz, although it finds two sources at lower frequency. CLEAN-SC has the expected problem of finding sources in between the two speakers at low frequency. The frequency for successful separation is unclear, but no lower than 4500 Hz. LP arguably has the best resolution, but it does have a problem with multiple spots. Figure 5g), FB with $\nu = 500$, was added to show that FB can separate the sources over 3187-3750 Hz, but the range of 3937-4500 Hz seems to be intractable for FB in this data. The right source has fallen below the 10 dB scale of the plot in Fig. 5g) at the highest two frequencies shown.

Setting ν too high alters the relative levels of the sources in FB, but RAB does not seem to detect the 3 dB level difference at all. Two small Regions of Interest are shown in Fig. 6a). Source spectra were determined by finding the peak level seen in the Left ROI and the Right ROI for each frequency. The difference Right - Left is the plotted in Fig. 6b) to show the difference that the method sees between the sources. The expected value is -3 dB. FDBF and FB with $\nu = 10$ and 30 all track -3 dB at high frequency. FB has considerable scatter in the range of 6-8 kHz. The curve for $\nu = 100$ is not shown because it goes off the scale in this frequency range. At the low frequency end, FB detects the second speaker and the curves move downward at lower frequency than FDBF. RAB does not produce the correct level difference.
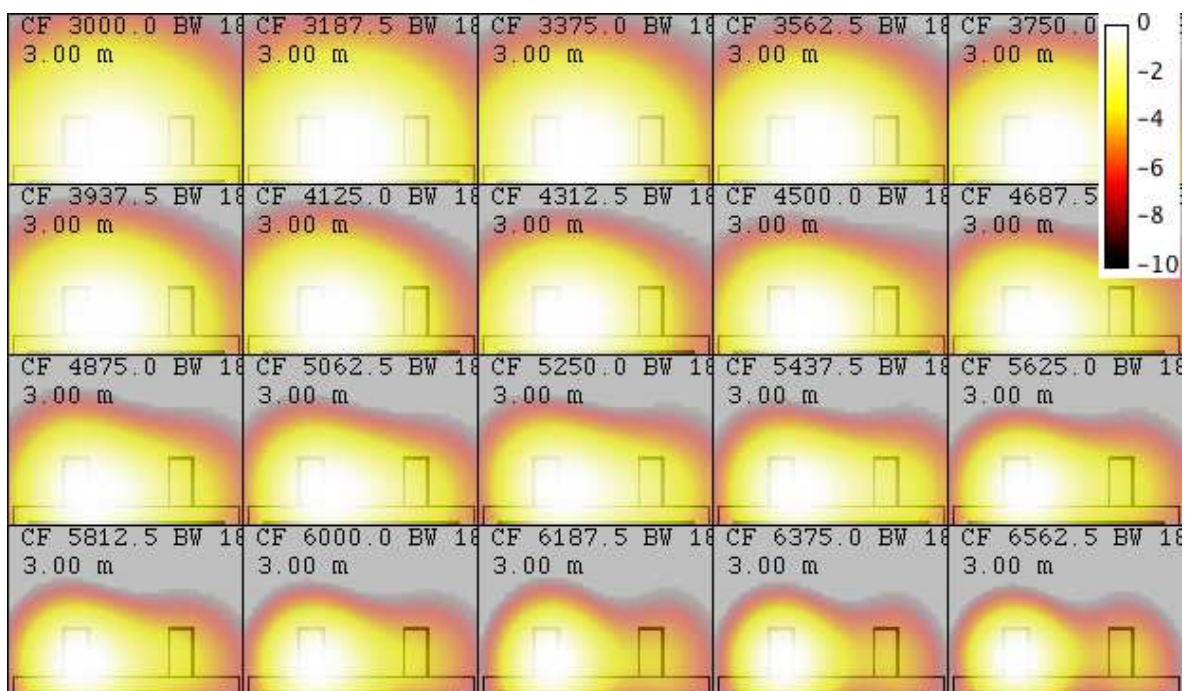

Fig. 5a). Resolution test using FDBF. 0.5 m speaker spacing, 3 dB level difference, 5 m distance, 0.35 m aperture. Rayleigh limit = 5030 Hz. 10 dB scale.
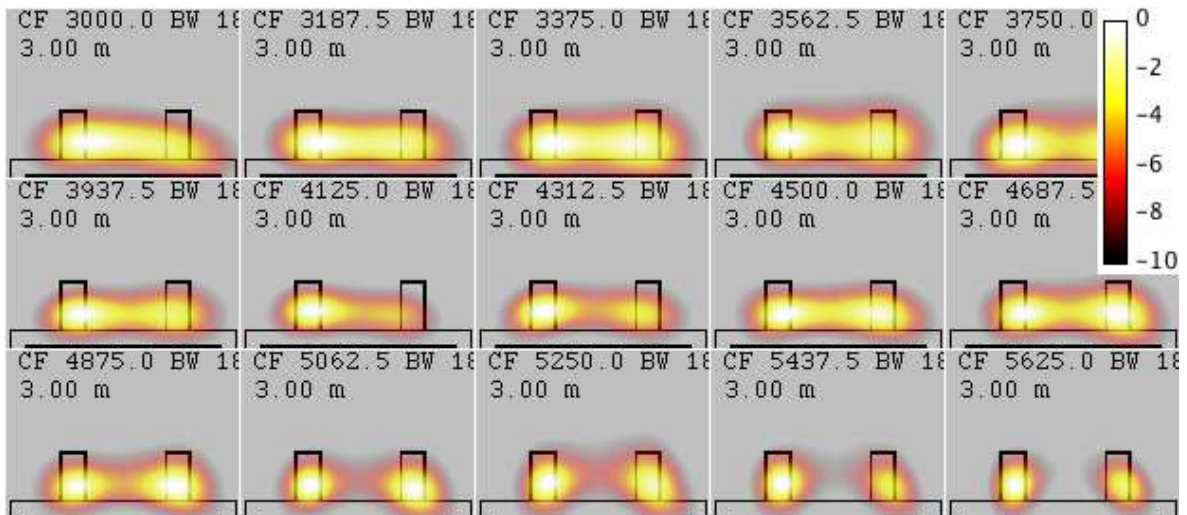
Fig. 5b). Resolution test using Robust Adaptive Beamforming. Diagonal loading parameter, $\lambda = 0.01$. Speaker spacing = 0.5 m. Distance = 5 m. Speaker level difference = 3 dB. Rayleigh limit frequency = 5030 Hz. Plotting scale = 10 dB.
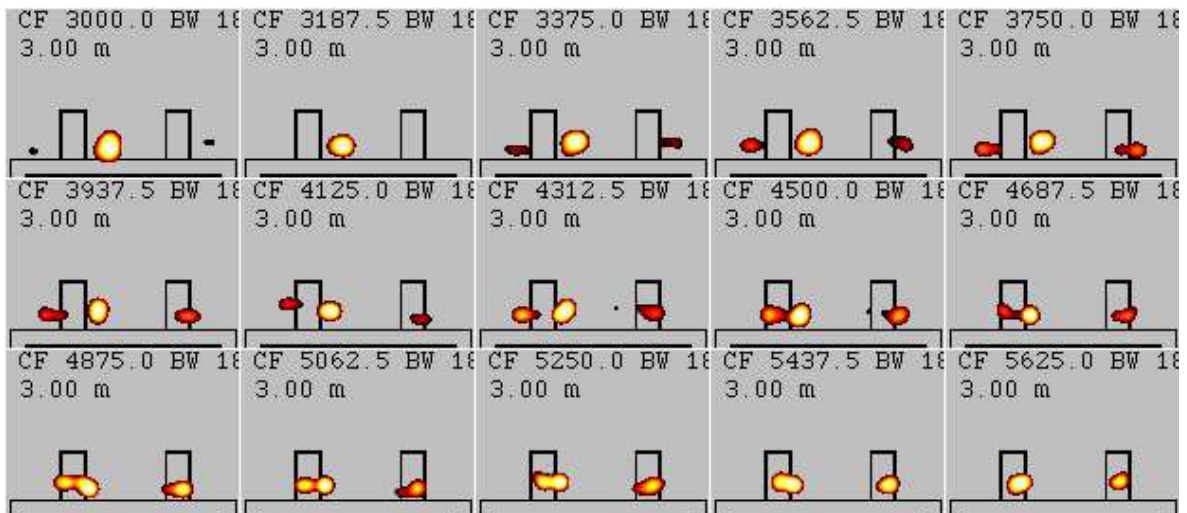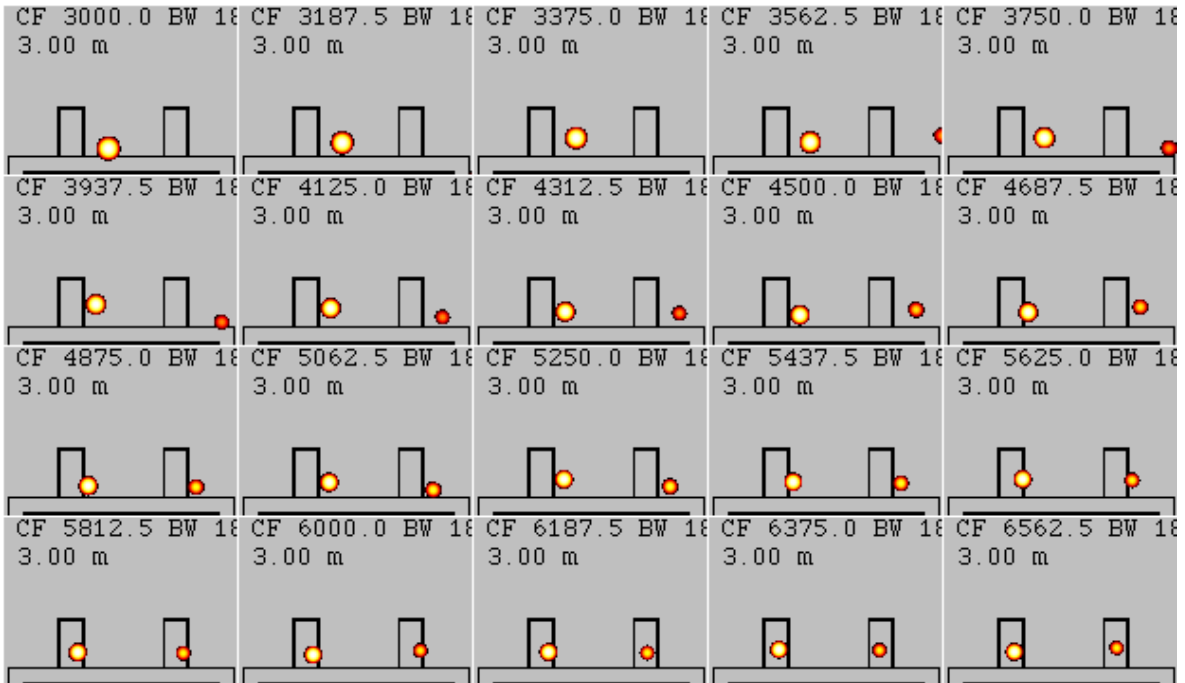

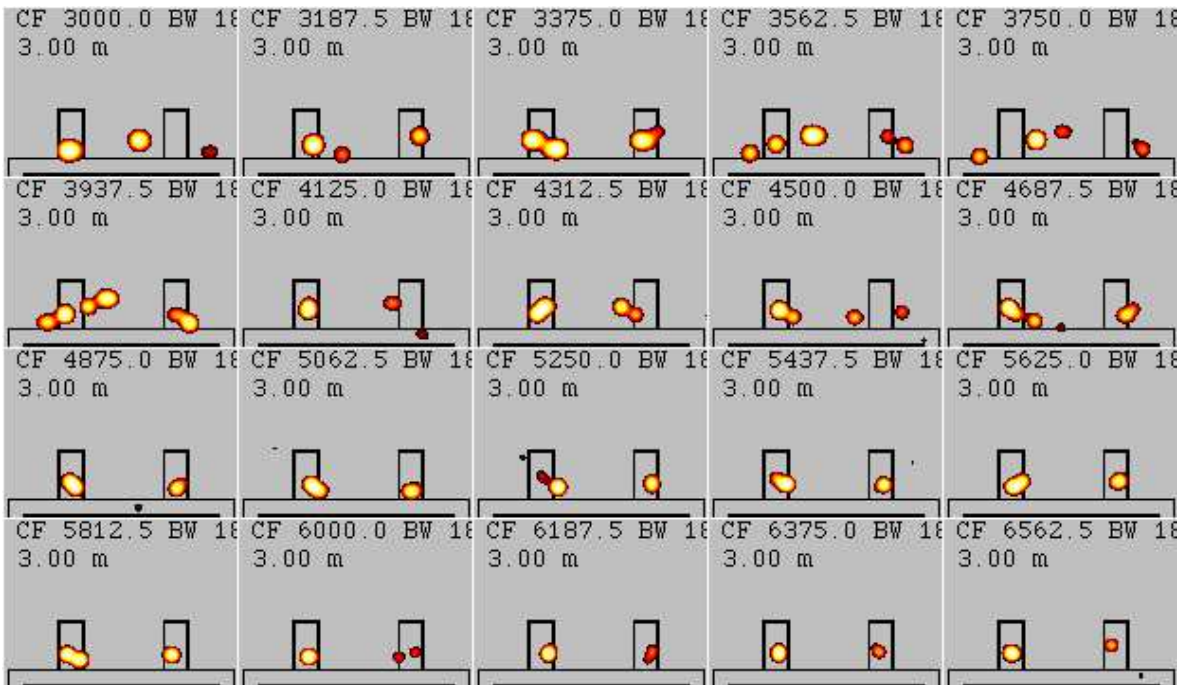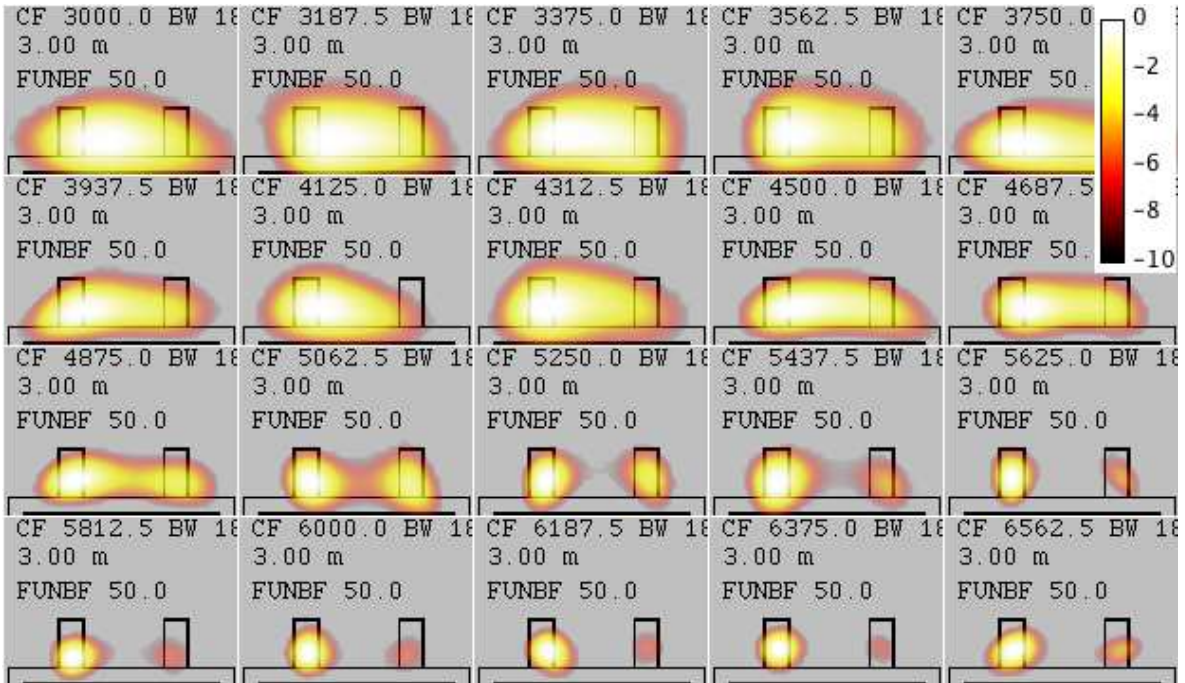*Fig. 5c). Resolution test using CLEAN-SC. Safety factor, $\varphi = 0.1$. Speaker spacing = 0.5 m. Distance = 5 m. Speaker level difference = 3 dB. Rayleigh limit frequency = 5030 Hz. Plotting scale = 10 dB.*

*Fig. 5d). Resolution test using Orthogonal Beamforming. Eigenvalues plotted = 10. Speaker spacing = 0.5 m. Distance = 5 m. Speaker level difference = 3 dB. Rayleigh limit frequency = 5030 Hz. Plotting scale = 10 dB.*

Fig. 5e). Resolution test using Linear Programming. Speaker spacing = 0.5 m. Distance = 5 m. Speaker level difference = 3 dB. Rayleigh limit frequency = 5030 Hz. Plotting scale = 10 dB.

Fig. 5f). Resolution test using Functional Beamforming. Order $\nu = 50$. Speaker spacing = 0.5 m. Distance = 5 m. Speaker level difference = 3 dB. Rayleigh limit frequency = 5030 Hz. Plotting scale = 10 dB.
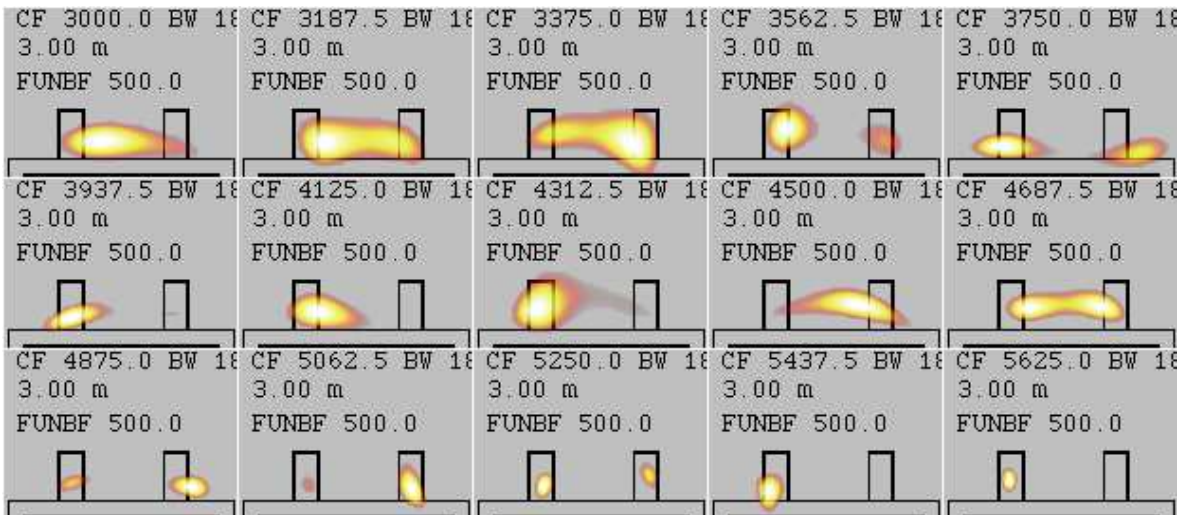
Fig. 5f). Resolution test using Functional Beamforming. Order $\nu = 500$.
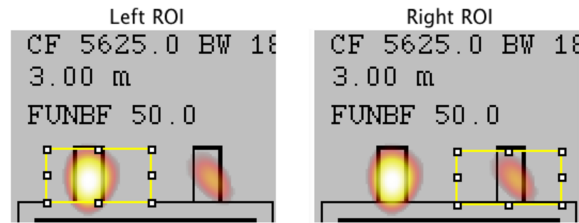
Figure 6a). The Left and Right Regions of Interest used for estimating speaker source strength from beamform maps. The maximum level in the ROI is found for each frequency.
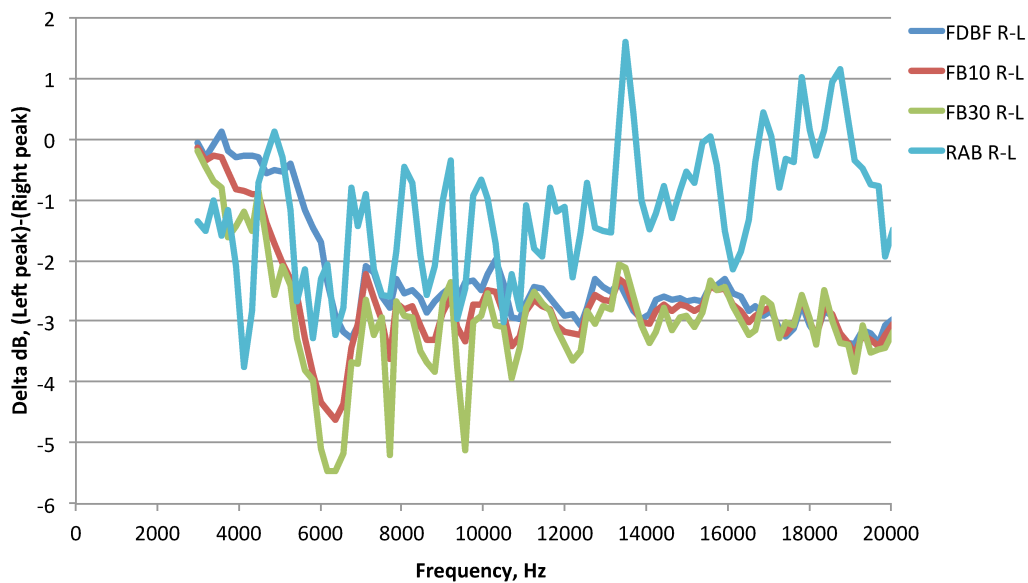

Fig. 6b). Level of left speaker source relative to right speaker source estimated by beamforming. Curves for FDBF, Functional Beamforming with $v = 10$ and 30, and Robust Adaptive Beamforming are shown. The expected result is -3 dB.

3.3   Dynamic range test

To investigate the dynamic range capability of the methods, the process described in the previous section was repeated with the $x = 0.5$ m speaker CSM reduced in level by 30 dB relative to the $x = 0$ speaker. This produces a challenging test to detect a very weak source. Plots from FDBF, RAB, CLEAN-SC, OB, and FB are shown in Fig. 7. It can be seen that Functional Beamforming detected the weak source, and none of the other methods did. Relative level spectra using peak values in the ROIs in Fig. 6a), are shown in Fig. 8 for FDBF and Functional Beamforming for $v = 10$, 30, 100 and 200. The higher v values can begin to measure the weak source at lower frequency, but are increasingly unstable in the range of 5-12 kHz and above 17 kHz. All four of the FB orders give very good results over 12-17 kHz.
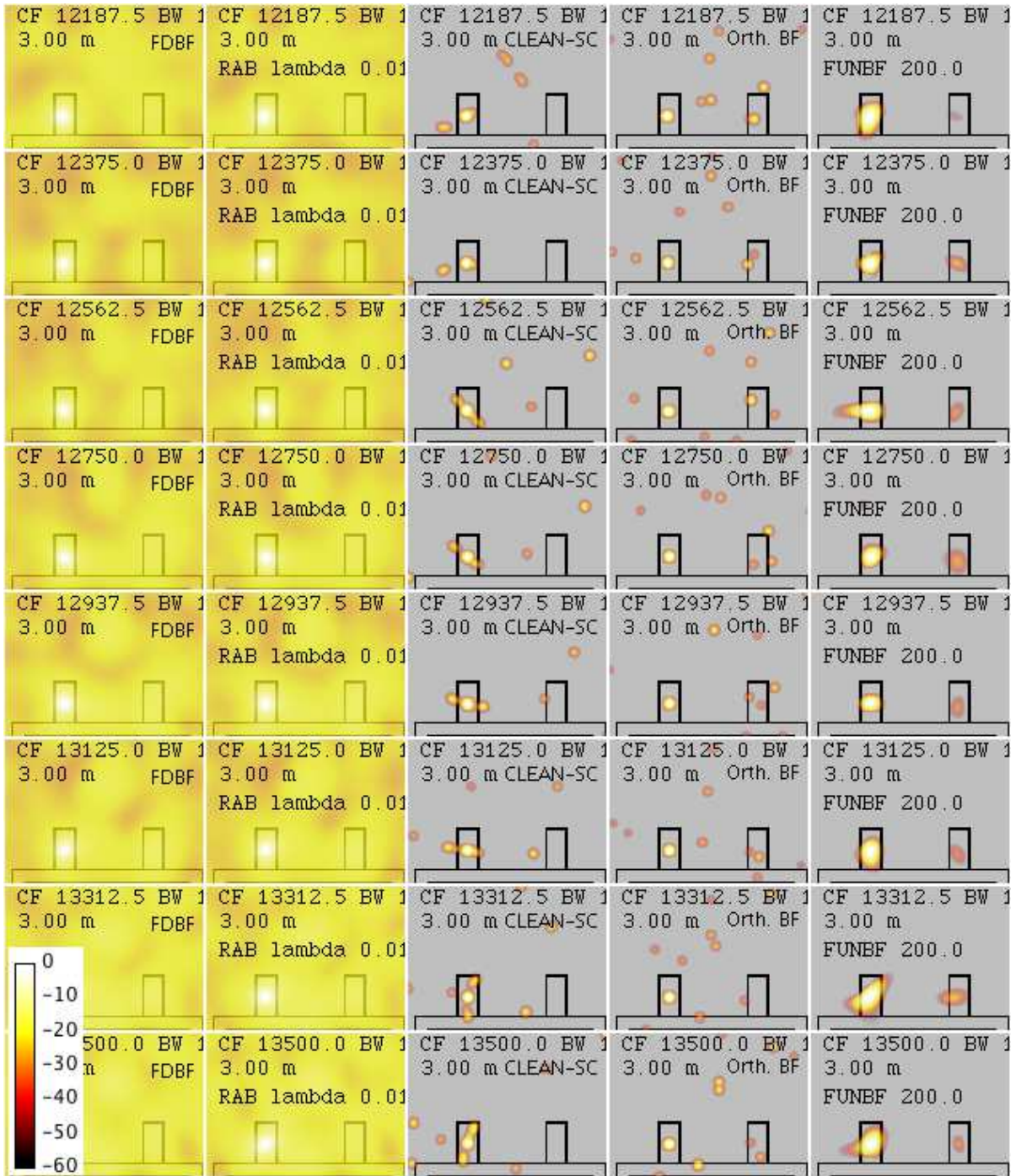
Fig. 7. Beamforming to detect a weak source (-30 dB) located 0.5 m from the stronger source at a distance of 3 m using Array 24 Jr. Left to right: FDBF, Robust Adaptive Beamforming, CLEAN-SC, Orthogonal Beamforming, and Functional Beamforming.
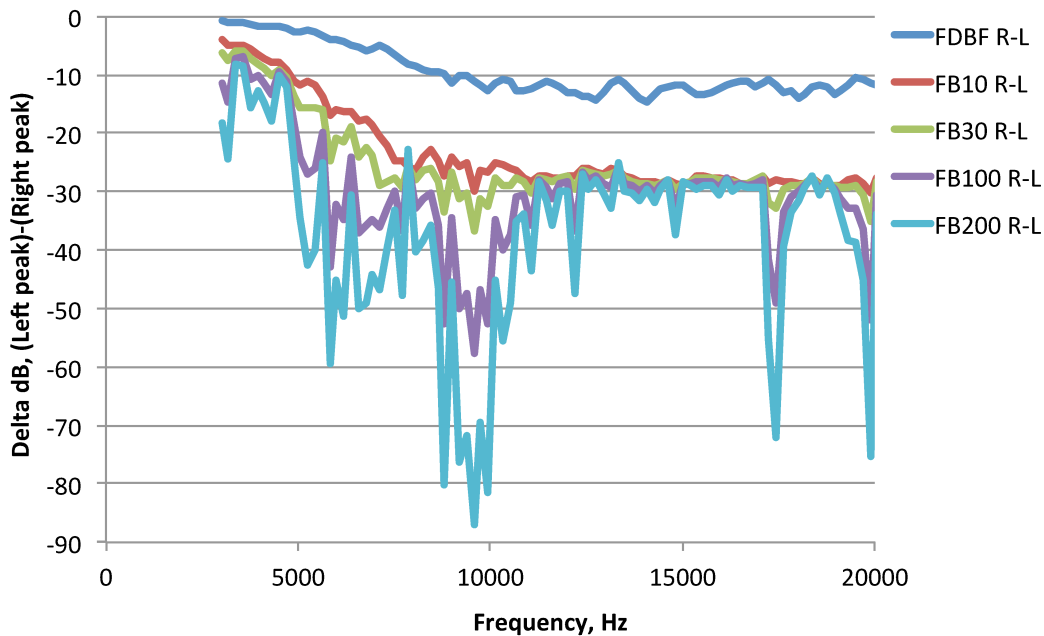
Fig. 8. Level of left speaker source relative to right speaker source estimated by beamforming FDBF and Functional Beamforming with v = 10, 30, 100 and 200. The expected result is -30 dB. Array 24 Jr, 3 m away from the sources, which are separated by 0.5 m.

3.4   Detecting a weak source in the presence of an extended source.

A small speaker was mounted on a pole and used to measure 18 data sets by moving the pole along a line from x = -0.85 m to +0.85 m at increments of 0.1 m. The line was parallel to and 3 m away from Array 24 Jr. Starting from the second CSM, the data files were successively scaled by -1.76 dB relative to the previous file so that the 18th CSM became 30 dB below the first file. The CSMs were summed to approximate a nonuniform line source, simulating what might be expected from jet mixing noise or the trailing edge of a wind turbine blade. In addition, the pole was shortened and used record a 19th CSM with the speaker located roughly at $x = 0, y = -0.5$ m. This file was scaled to be 25 dB below the total of the line source. One of the individual speaker datasets was used to compute a new calibration because the calibration for the table-speaker data discussed previously was measured 17 months before the pole data.

Results for FDBF and RAB at 12750 Hz are shown in Fig. 9. The background photographic image shows the first and last pole location and the lower speaker location. On a 10 dB scale, the FDBF plot is similar to a typical jet noise beamforming plot. Changing to RAB reduces the sidelobes, improves the resolution and shows more of the source. The lower speaker is not seen, of course, because it is below the scale in level. Increasing the range of the scale shows a floor in both cases, and does not reveal the lower speaker. Plots on a 60 dB scale for CLEAN-SC, OB, and FB with v = 100 and 300 are given in Fig. 10. CLEAN-SC and OB show the extended source as dots, but these dots are not the locations of the speakers. OB may have detected the lower source. Functional Beamforming clearly detects it, and shows the extended source as a continuous image. The frequency is too low to resolve the

individual speakers of the line. Increasing ν reduces the sidelobes. Higher frequency results (25 kHz) are shown in Fig. 11, but the individual speakers are still not resolved.

The effect of calibration is explored in Fig. 12, which gives the FB results with $\nu = 300$ using a) the old calibration (which is also a different speaker type) and b) no calibration. The results are degraded compared with Fig 10d), but the lower speaker is still seen.
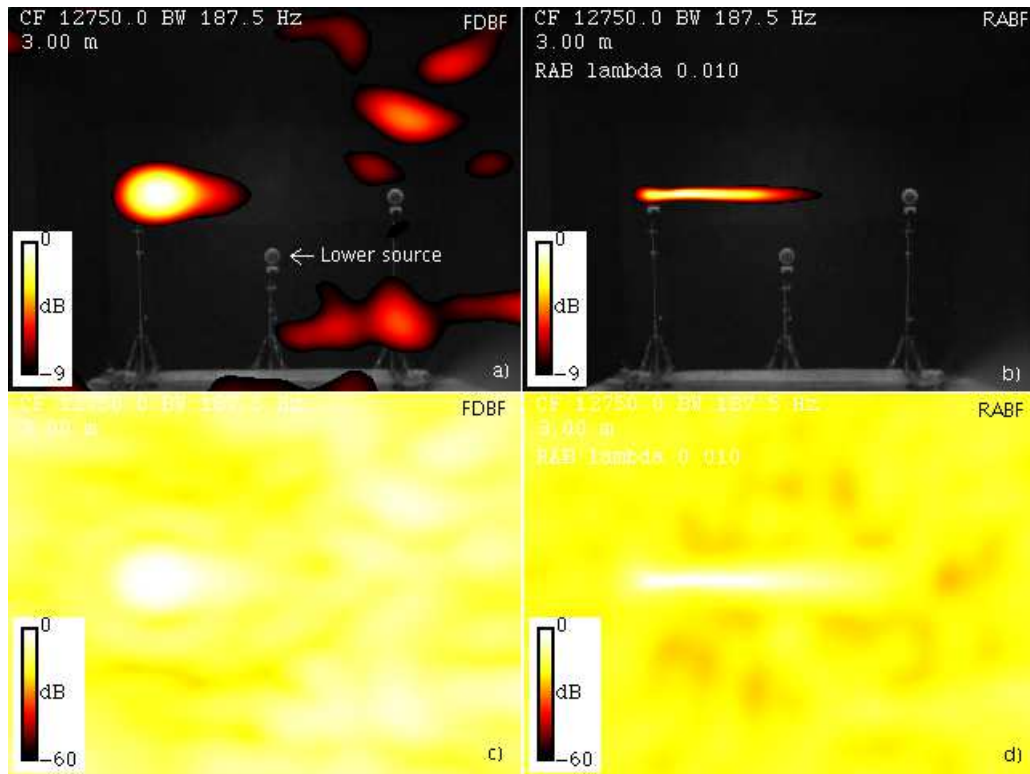

Fig 9. An extended source and a lower source at a level 25 dB below the extended source. 12750 Hz. a) FDBF on a 10 dB scale. b) Robust Adaptive Beamforming on a 10 dB scale. c) FDBF on a 60 dB scale. d) Robust Adaptive Beamforming on a 60 dB scale.
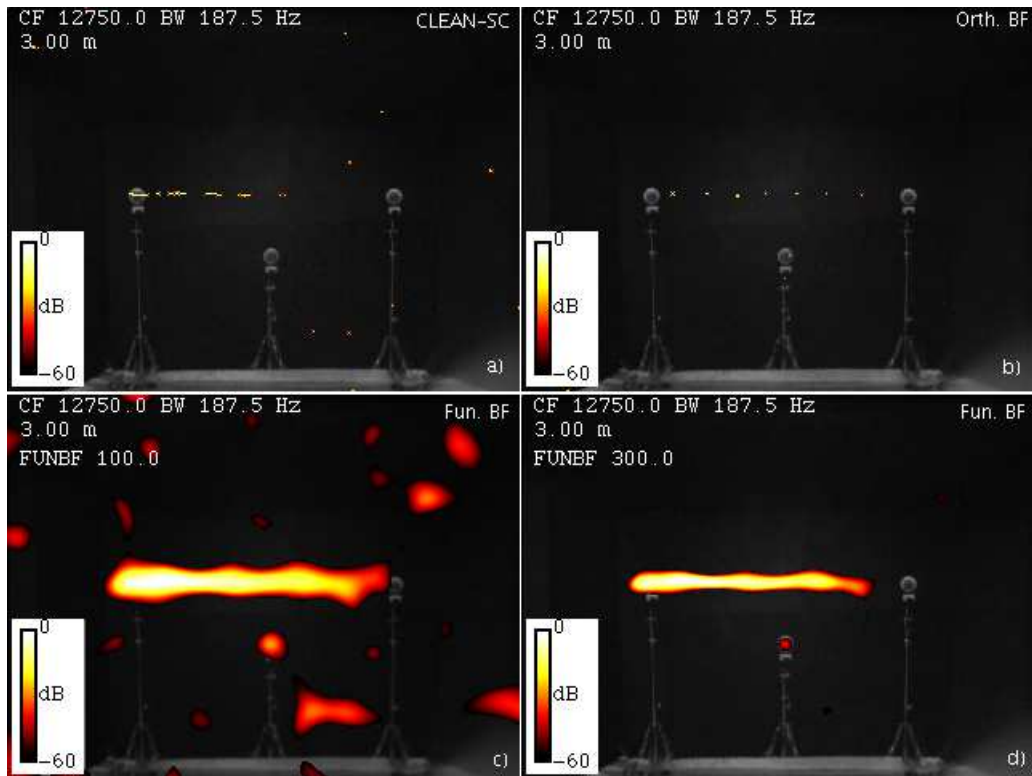
Fig. 10. An extended source and a lower source at a level 25 dB below the extended source. 60 dB scale. 12750 Hz. a) CLEAN-SC. b) Orthogonal Beamforming. c) Functional Beamforming with $\nu = 100$. d) Functional Beamforming with $\nu = 300$.
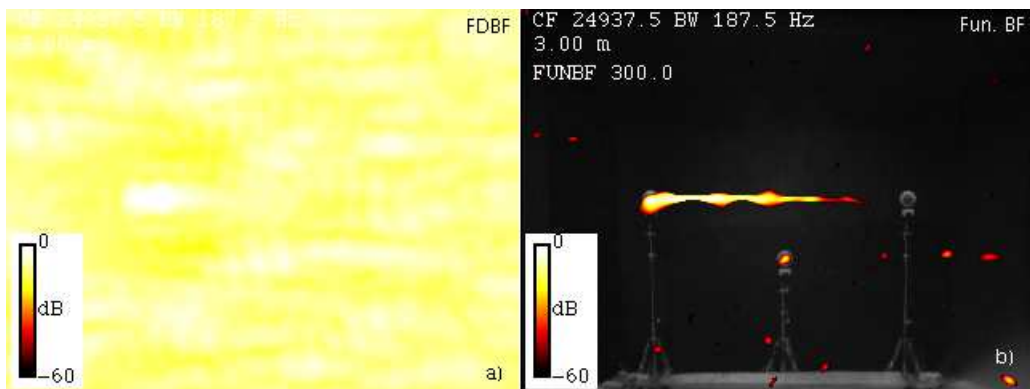

Fig. 11. An extended source and a lower source at a level 25 dB below the extended source. 60 dB scale. 25 khz Hz. a) FDBF . b) Functional Beamforming with $\nu = 300$.
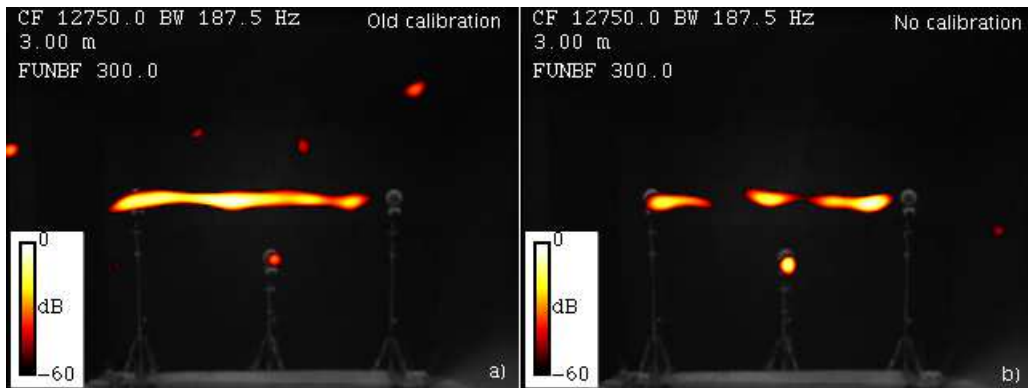
Fig 12. An extended source and a lower source at a level 25 dB below the extended source. 60 dB scale. 12750 Hz. Functional Beamforming with $v = 300$. a) Using an old speaker calibration that employed a different type of speaker. b) Using no calibration. The case with the current calibration is shown in Fig. 10 d).

3.5 Non-speaker data

Functional beamforming has been applied to a number of datasets since it was discovered a few months ago. In almost every case, new sources have been found lurking below the dynamic range limit of the methods previously available. A few examples are given here.

The jet shown in Fig. 1 was used for Fig. 13 (4875 Hz). The extent of the source is not seen with conventional beamforming.

A very simple aerodynamic noise source is shown in Fig. 14. Details of the leading edge noise caused by impingement of turbulence in the shear layer and trailing edge noise are seen. Compare with Ref. [5].

Fig. 15 is a reanalysis of an old dataset imaging a bridge using Array 24. Functional Beamforming shows higher dynamic range results. No calibration was available.

A desk model of a Boeing 747-8 was subjected to the low speed jet to simulate an airframe noise test. As shown in Fig. 16, FB detected a very subtle feature of the model design.
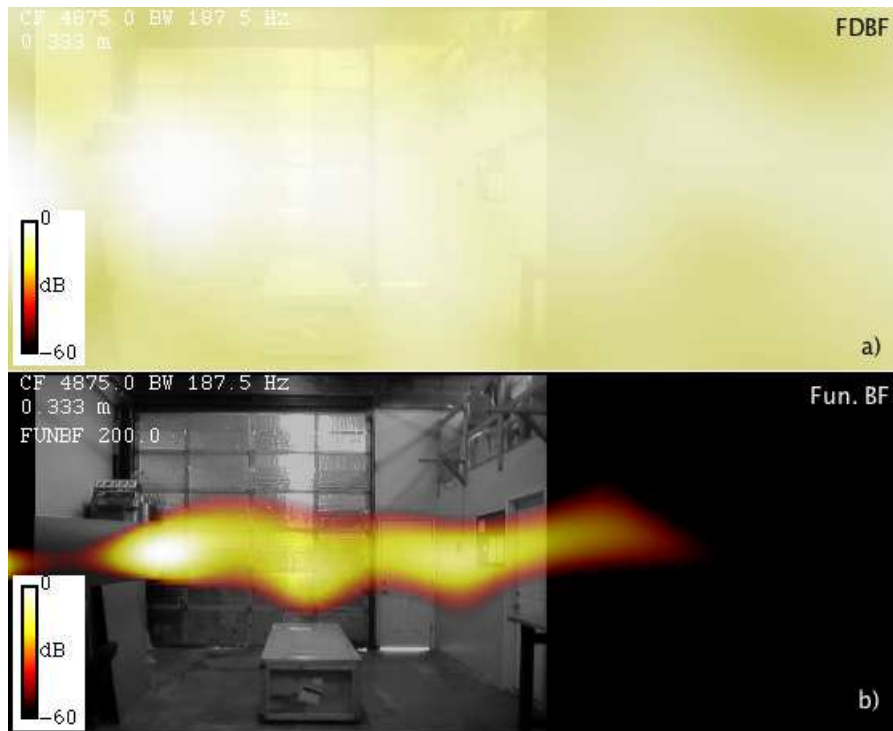
Fig. 13. A Mach 0.15 jet imaged at 4875 Hz with a) FDBF and b) Functional Beamforming.
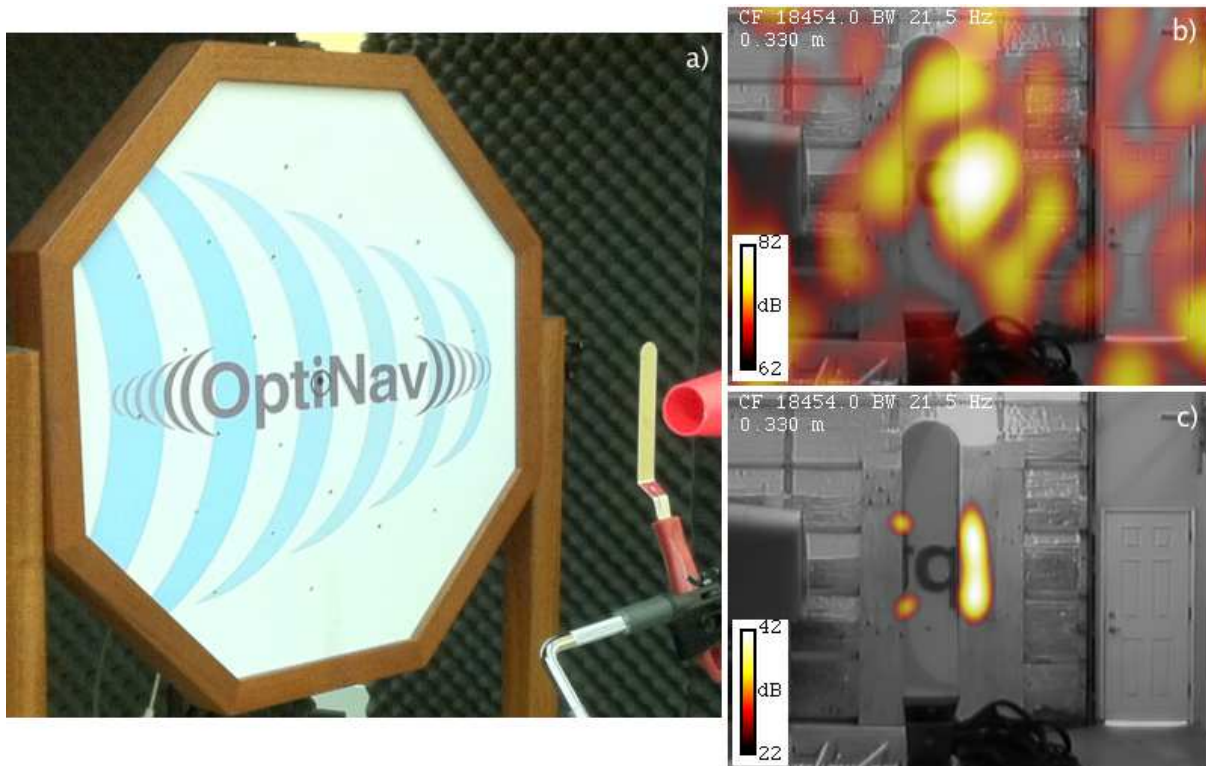

Fig. 14. Spatula leading and trailing edge noise. 0° AOA. 18.5 kHz, a) Setup with Array 24 Jr., b) FDBF, c) Functional beamforming.
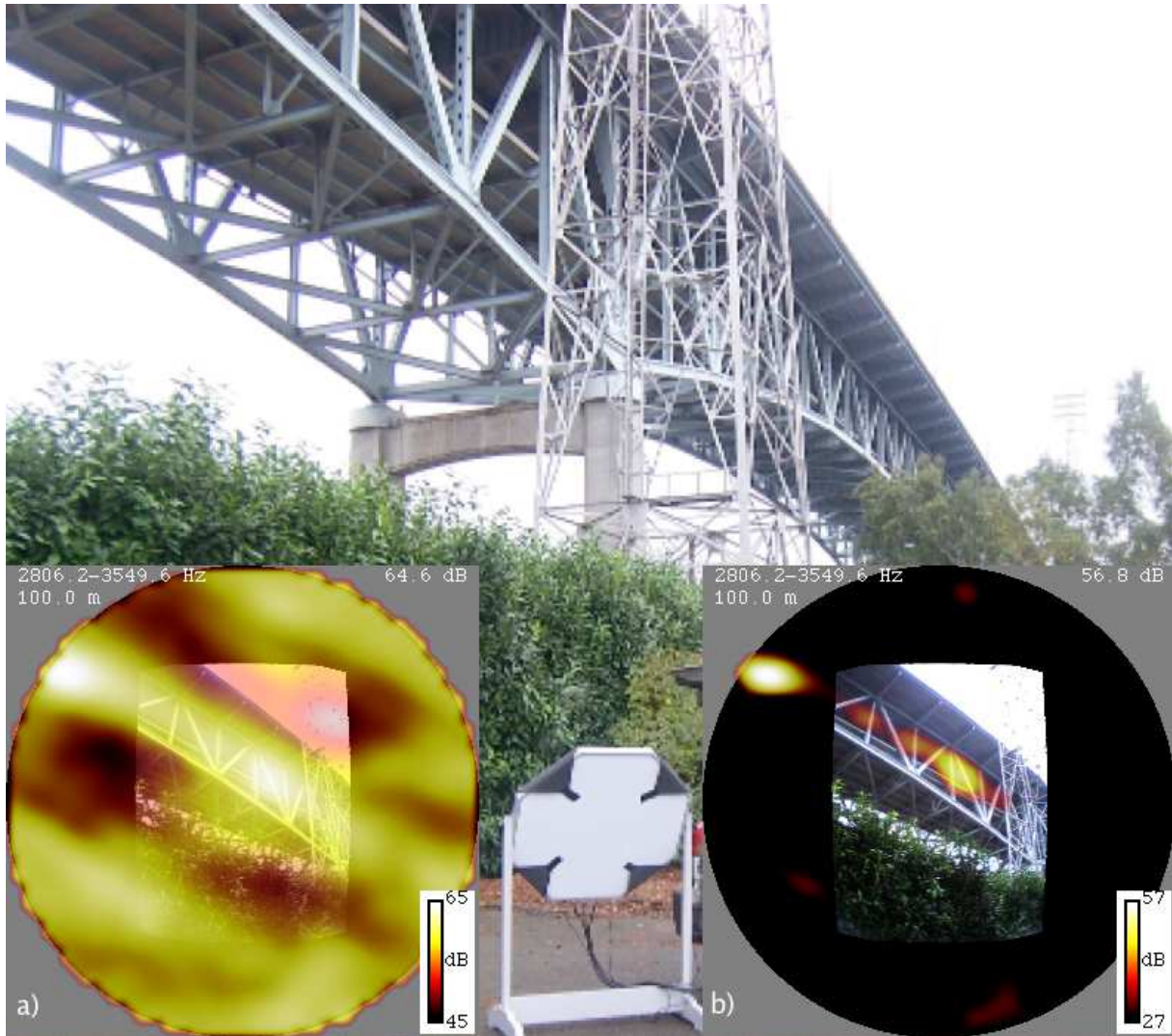
Fig. 15. Noise from a double deck bridge. Sound from traffic on the lower (express lanes) deck reflects from the bottom of the upper deck. Array 24. 2.8 kHz. a) FDBF, b) Functional beamforming.

Fig. 16. Functional Beamforming of Airframe noise from a desk model of a Boeing 747-8. The spots near the leading edge of the wing root are from tiny depressions representing the air cycle machine inlets.

4   CONCLUSIONS

Functional Beamforming (BF) is a simple modification of conventional Frequency Domain Beamforming that offers much higher dynamic range than FDBF or any other beamforming method to the author's knowledge. Dynamic range of more than 30 dB has been demonstrated over a substantial bandwidth using a 24-element array with inexpensive microphones. FB has no significant impact on computing time or other resources. It depends on an order, ν, that connects it with FDBF ($\nu = 1$) and even MVDR ($\nu = -1$). The resolution of FB is better than that of FDBF, but not quite as sharp as Robust Adaptive Beamforming or Linear Programming. Unlike deconvolution methods, it shows continuous source distributions as continuous images. There is a proof of its quantitative nature based on the theory of matrix monotone functions. If the steering vector is correct, FB will never give a result that is lower than the actual source strength. Furthermore, the beamform map steadily decreases as ν is increases. The sidelobes gradually disappear and the main lobes become somewhat narrower. At first glance, this would seem to suggest that that the exact answer is obtained in the limit as $\nu \rightarrow \infty$, but this is unproven and seems too good to be true. In practice, errors in array calibration or the propagation model will cause at least small errors in the computed steering vectors, and this will limit the useful range of ν. Experience to date suggests that an uncalibrated array can support ν up to 30 and a well-calibrated one can handle ν in the hundreds.

REFERENCES

[1]   Brooks, T.F. and W.M. Humphreys, Jr. "A Deconvolution Approach for the Mapping of Acoustic Sources (DAMAS) determined from phased microphone arrays," AIAA Paper 2004-2954, 2004.

[2]   Dougherty ,R.P., R.C. Ramachandran and G.Raman,"Deconvolution of Sources in Aeroacoustic Images from Phased Microphone Arrays Using Linear Programming," R.P., AIAA Paper 2013-2210, Berlin, Germany, 2013.

[3] P. Sijtsma. "CLEAN based on spatial source coherence." Int. J. Aeroacoustics, 6, 357–374, 2007.

[4] Dougherty, R.P., "Source Location with Sparse Acoustic Arrays; Interference Cancellation," CEAS-ASC Workshop, "Wind Tunnel Testing in Aeroacoustics" DNW, Noordoostpolder, the Netherlands, November 5-6, 1997.

[5] Sarradj, E., "A fast signal subspace approach for the determination of absolute levels from phased microphone array measurements," Journal of Sound and Vibration 329, 1553–1569, 2010.

[6] Cox, H., R. M. Zeskind, and M. M. Owen, "Robust adaptive beamforming," IEEE Trans. Acoust., Speech, Signal Process., 35 (10), 1365–1376, 1987.

[7] Johnson, D. H. and Dudgeon, D.E., *Array Signal Processing: Concepts and Techniques* Prentice-Hall, 1993.

[8] Huang X., L. Bai, I.Vinogradov, and E. Peers, "Adaptive beamforming for array signal processing in aeroacoustic measurements," J Acoust Soc Am. 131(3), 2152-61, 2012.

[9] Underbrink, J.R., and R.P. Dougherty, "Array design for non-intrusive measurement of noise sources," Noise-Con 96, Bellevue, WA, 1996.

[10] Bhatia, R., Matrix Analysis (Graduate Texts in Mathematics), Springer, 1997.

[11] Witkowski, A., "A new proof of the monotonicity of power means," Journal of Inequalities in Pure and Applied Mathematics, Vol. 5, Issue 1, Article 6, 2004.